Review

International Journal of Modern Physics A
Vol. 28, No. 8 (2013) 1330012 (20 pages)

DOI: 10.1142/S0217751X13300123

World Scientific
www.worldscientific.com

# MONOJET EVENTS: FROM DARK MATTER TO EXTRA DIMENSIONS, A SEARCH FOR THE EXOTICS USING THE STANDARD MODEL

PIERRE-HUGUES BEAUCHEMIN

*Department of Physics and Astronomy, Tufts University, 212 College Ave, Medford, MA 02155, USA*
*Hugo.Beauchemin@tufts.edu*

REYHANEH REZVANI

*Department of Physics, University of Toronto, 60 St. George St, Toronto, ON, Canada M5S 1A7*
*reyhaneh.rezvani@cern.ch*

Received 10 February 2013
Accepted 18 February 2013
Published 20 March 2013

Monojet events consist in event topologies with a high transverse momentum jet and a large amount of missing transverse energy. They constitute a promising final state that could lead to phenomena beyond the Standard Model. The theoretical models giving rise to such a signature include the pair production of Weakly Interacting Massive Particles, as dark matter candidates, and models of large extra dimensions. Monojet events can even be used to measure the Standard Model properties of $Z$ boson decays, provided that the precision of the analysis is high enough. Such precision can be achieved by using data-driven determinations of the Standard Model contributions to monojet events. Exotics searches for new physics in such a final state have been performed at all high energy hadronic collider experiments since SPS. The ATLAS and CMS analyses with 7 TeV LHC data provide the latest and most useful information obtained from monojet studies. Their results are presented and discussed in this review paper.

*Keywords*: ATLAS detector; CMS detector; exotics; monojet.

PACS numbers: 13.85.−t, 29.85.Fj, 12.60.−i, 95.35.+d

## 1. Introduction

Event topologies with one high transverse momentum jet and a large amount of missing transverse energy $E_T^{\text{miss}}$, classified as monojet events, are specific to hadron colliders. Due to the strong interaction involved in the production mechanism of such a final state, many new physics scenarios predict a substantial rate (of $\mathcal{O}(1)$ pb) for such events in a wide unexplored region of their parameter space. The large $E_T^{\text{miss}}$ in such events suppresses the otherwise dominant QCD multijet background

typical at hadron colliders. Searching for phenomena beyond the Standard Model (BSM) in monojet events therefore provides a high discovery potential at the LHC. These events can also be used to measure the new physics couplings in the case where a discovery is made in other channels (see for example Allanach and Grab's paper[1]). In the case of an agreement between the observed monojet events and the Standard Model (SM) expectations, constraints can be set on the parameters of the new physics models predicting such event topologies. Monojet events could also be used to measure the parameters of the SM at the LHC. In particular, a precise, direct measurement of the invisible partial decay width of the $Z$ boson, $\Gamma_Z(\text{inv})$, could be performed using monojet events. Because of their expected sensitivity to SM and BSM physics, careful study of monojet events is an important aspect of hadron collider physics programs.

### 1.1. *Probing physics in monojet events*

Astrophysical observations of dark matter[2] provide one of the strongest motivations for physics BSM accessible at the LHC.[3] The nature of dark matter can consist in Weakly Interacting Massive Particles (WIMPs).[4] These WIMPs would not leave any electronic signal in a high energy physics detector. Their existence would need to be inferred from the particles recoiling them in a collider event. In the popular cold dark matter scenario,[5] such particles are stable. A new discrete symmetry must thus protect them from decaying to lighter SM particles. As a consequence, dark matter candidates would be produced in pairs at the LHC, possibly leaving no signal to detect events in which they would be directly produced from the annihilation of a pair of gluons or a quark and an antiquark. However, the initial particles also have a high probability of emitting a final state parton with large momentum before the collision happens (initial state radiation). In such generic scenario, dark matter production at the LHC would therefore result in two WIMPs plus a parton final state, thus yielding the detectable monojet signature.

Various BSM models predict the existence of dark matter candidates. For example, in supersymmetric versions of the SM, the production of dark matter candidates arises as a consequence of the R-parity symmetry introduced to prevent proton decay and also the decay of the lightest supersymmetric particle, the neutralino.[6,7] In little Higgs models,[8] the T-parity conservation is responsible for the stability of the massive particles that are dark matter candidates. In the Universal Extra Dimensions (UED) models,[9,10] SM particles are free to propagate in the bulk of femtometer size extra dimensions, leading to massive copies of the known quarks and gluons, the Kaluza–Klein modes, which can also decay to final states containing jets. The conservation of the Kaluza–Klein number, i.e. conservation of the momenta of the particles propagating in the extra dimensions, is the symmetry responsible for the prediction of a dark matter candidate in this theory. The phenomenology is very similar to that predicted by the Minimal Supersymmetric Model (MSSM).

Table 1. Operators coupling Dirac WIMP fermions to SM quarks or gluons.

| Name | Operator | Name | Operator |
|---|---|---|---|
| D1 | $\frac{m_q}{(M^\star)^3}\bar{\chi}\chi\bar{q}q$ | D2 | $\frac{m_q}{(M^\star)^3}\bar{\chi}\gamma^5\chi\bar{q}q$ |
| D3 | $\frac{m_q}{(M^\star)^3}\bar{\chi}\chi\bar{q}\gamma^5 q$ | D4 | $\frac{m_q}{(M^\star)^3}\bar{\chi}\gamma^5\chi\bar{q}\gamma^5 q$ |
| D5 | $\frac{1}{(M^\star)^2}\bar{\chi}\gamma^\mu\chi\bar{q}\gamma_\mu q$ | D6 | $\frac{1}{(M^\star)^2}\bar{\chi}\gamma^\mu\gamma^5\chi\bar{q}\gamma_\mu q$ |
| D7 | $\frac{1}{(M^\star)^2}\bar{\chi}\gamma^\mu\chi\bar{q}\gamma_\mu\gamma^5 q$ | D8 | $\frac{1}{(M^\star)^2}\bar{\chi}\gamma^\mu\gamma^5\chi\bar{q}\gamma_\mu\gamma^5 q$ |
| D9 | $\frac{1}{(M^\star)^2}\bar{\chi}\sigma^{\mu\nu}\chi\bar{q}\sigma_{\mu\nu}q$ | D10 | $\frac{1}{(M^\star)^2}\epsilon^{\mu\nu\alpha\beta}\bar{\chi}\sigma^{\mu\nu}\gamma^5\chi\bar{q}\sigma_{\alpha\beta}q$ |
| D11 | $\frac{1}{(4M^\star)^3}\bar{\chi}\chi\alpha_s(G^a_{\mu\nu})^2$ | D12 | $\frac{1}{(4M^\star)^3}\bar{\chi}\gamma^5\chi\alpha_s(G^a_{\mu\nu})^2$ |
| D13 | $\frac{1}{(4M^\star)^3}\bar{\chi}\chi\alpha_s G^a_{\mu\nu}\tilde{G}^{a,\mu\nu}$ | D14 | $\frac{1}{(4M^\star)^3}\bar{\chi}\gamma^5\chi\alpha_s G^a_{\mu\nu}\tilde{G}^{a,\mu\nu}$ |

Predictions from these theories strongly depend on the values of multiple parameters added to the already long list of SM free parameters. A general and less model-dependent approach to WIMP production can be adopted using the effective theory formalism.[11–13] In such a scenario, the interactions between the dark matter sector and SM particles involve mediators which are very heavy compared to the typical final state momenta of dark matter candidates at the LHC. This allows for a reliable description of the production of a pair of WIMPs from colliding partons using a simple contact interaction Lagrangian, valid well below the mass scale of the heavy mediators. Assuming that the WIMP particles are Dirac fermions,[a] 14 different effective operators can be considered for such contact interactions, depending on the Lorentz structure of the SM and WIMP fermion currents composing the operators. Table 1 lists these operators following the naming scheme established by Goodman *et al.*[14] The parameter $M^*$ corresponds to the mass of a heavy mediator divided by its couplings to partons and to WIMPs, $M^* = \frac{M}{\sqrt{g_q g_\chi}}$. This parameter is equivalent to the compositeness scale in theories where an underlying structure for quarks is considered,[15,16] and is the parameter to be constrained by the experiment. Limits on this parameter are set for each assumed mass of the dark matter candidates, in case no deviation with respect to the SM prediction is observed in data.

These interactions can be further classified into five categories based on their missing transverse energy distributions. The operators D1, D5, D8, D9, D11 represent each of these categories. Operators of the same category cannot be disentangled experimentally in monojet events. While operators D1, D5, D8 and D9 describe different quark couplings (vector, axial vector and scalar couplings) to

[a]The only difference for Majorana fermions would be that certain interaction types are not allowed and the cross-section for each operator is larger by a factor of four.

WIMPs ($qq \to \chi\bar{\chi}$), D11 describes the gluon coupling ($gg \to \chi\bar{\chi}$). Tests of this generic dark matter scenario must therefore be carried out separately for each of the operators. However, more than one operator can contribute to the dark matter production if WIMPs provide the correct explanation to the observed amount of dark matter in the universe.

Other theoretical frameworks also suggest that monojet events provide potential for discovery, one of the most popular being the large extra dimensions scenario of Arkani-Hamed, Dimopoulos, Dvali (ADD).[17] Extra dimensions could constitute an important ingredient to a solution to the hierarchy problem in an attempt to explain why gravity is so much weaker than the other forces. In the ADD scenario, gravity propagates in the $(4 + n)$-dimensional bulk of space–time where $n$ is the number of extra spatial dimensions, while the SM fields are confined to our usual four dimensions. By comparing Newton's law of gravity in the four-dimensional perspective with its $(4 + n)$-dimensions equivalent, the fundamental characteristic mass scale of gravity, $M_D$, can be related to the effective Planck mass $M_P$: $M_P^2 \sim M_D^{2+n} R^n$, where $R$ is the size of the extra dimensions. If the extra dimensions are large enough, the fundamental scale of gravity $M_D$ can be as low as the weak scale, hence eliminating any hierarchy between the observable Higgs mass and the size of its quantum corrections. The apparent weakness of gravity would then be due to its dilution in the bulk of the large extra dimensions. In addition, this would offer the unprecedented opportunity to study gravity in particle colliders, providing critical information on how to formalize a quantum description of gravity, one of the important elements missing in the SM. While there is no model of quantum gravity thus far, an effective field theory approach can be used to make predictions for direct graviton production in the context of the ADD scenario at energies below the fundamental Planck scale $M_D$. This is the context in which ADD predictions can be made for collider experiments.[18]

At hadron colliders, graviton modes would be produced in association with a jet via three processes: $qg \to qG$, $gg \to gG$ and $q\bar{q} \to gG$, where $G$ stands for a graviton state, $q$ for quark and $g$ for gluon. Gravitons do not interact with the detector due to the weakness of the gravitational force in four dimensions, or equivalently due to the propagation of the graviton field into the extra spatial dimensions that are much larger than the width of the graviton wave-packet. This would result in missing energy, and hence in a monojet signature.

If no new physics is observed, the monojet data can be used to perform SM measurements. Since the major SM contribution to these events comes from $Z(\nu\nu)$ + jets events, a direct measurement of the invisible decay width of the $Z$ boson can be performed. The idea is to exploit the large cancellation of systematic uncertainties related to the jet reconstruction and QCD modeling in the measurement of the ratio of $Z(\nu\nu)$ to $Z(\ell\ell)$ branching ratios, to obtain a measurement of the invisible width of the $Z$ with high precision, using $\Gamma_{Z(\ell\ell)}$ from the LEP measurement results. Such a measurement offers the opportunity to probe the weak couplings of $Z$ to neutrinos and to measure them in an hadronic environment. It

could also reveal anomalies not necessarily visible in BSM searches: the measurement is sensitive to any nonstandard couplings of the $Z$ boson to the SM neutrinos, or to any additional $Z$ decays to invisible exotic particles. Comparison of $Z(\nu\nu)$+jets events with $Z(\ell\ell)$ + jets events also provides an opportunity to study large angle QED final state radiation effects that modify the calorimeter jet clustering of the hadronic system recoiling from the $Z$ boson decaying to charged leptons. This can help to further improve the description of QED in particle generators, resulting in a reduction of the corresponding uncertainties in analyses with exclusive final state selections. While the SM physics that can be extracted from monojet studies is very interesting, it deserves a paper of its own and thus will not be further discussed in the following review.

### 1.2. *Monojet studies in hadron collider experiments*

Interests in monojet events sparked when the UA1 collaboration published the observation of an excess of such events over SM expectations in 1984.[19] Initially, this excess was interpreted as evidence for supersymmetry, however, it soon became clear that the excess was not consistent with supersymmetry expectations,[20,21] and could in fact be explained in terms of SM contributions.[22] In addition, no monojet excess was observed by the UA2 collaboration[23] so the interest for monojet events faded. Such interest, however, resurfaced in the late 90s after the proposal of using monojet events to search for large extra dimensions.[17,18] The first constraints on these models came from Tevatron Run I monojet analyses,[24,25] while the LHC potential for a discovery of extra dimensions was being investigated with Monte Carlo simulations.[26,27] In its first Run II monojet analysis,[28] the CDF collaboration developed a completely data-driven approach to determine the SM background which significantly reduced the main systematic uncertainties compared to the typical simulation-based predictions (for a review see Ref. 29). These techniques were extended and are now used as standard methods in the latest LHC monojet analyses.[30,31] CDF was also the first to combine monojet and monophoton analysis results to set the strongest limits on large extra dimension parameters,[32] and the first to use monojet events to constrain the generic dark matter scenario presented in the previous section.[33] However, because of the large data statistics and larger center-of-mass energy, LHC results rapidly superseded those obtained at the Tevatron. The present review will thus focus on the latest LHC analyses.

In the following, an overview of the searches for new physics in monojet events performed by the ATLAS and CMS collaborations at the LHC will be presented. First, a brief summary of the background determination will be provided, taking ATLAS predictions as an example. Then, the results of the 2011 ATLAS monojet analysis performed with 4.7 fb$^{-1}$ of integrated luminosity,[30] and of the CMS analysis corresponding to 5.0 fb$^{-1}$ of 7 TeV data[31] will be presented. They will be compared to the preliminary results of the 8 TeV ATLAS analysis performed with 10.5 fb$^{-1}$ of 2012 LHC data. These results will be interpreted in terms of large

Table 2. ATLAS and CMS monojet signal regions.

| | ATLAS | | CMS | |
|---|---|---|---|---|
| Signal region | $p_T$(jet 1) > | $E_T^{\text{miss}}$ > | $p_T$(jet 1) > | $E_T^{\text{miss}}$ > |
| Region 1 | 120 | 120 | 110 | 250 |
| Region 2 | 220 | 220 | 110 | 300 |
| Region 3 | 350 | 350 | 110 | 350 |
| Region 4 | 500 | 500 | 110 | 400 |

extra dimension models and generic dark matter scenarios. However, it is important to note that in order to have sensitivity to all current and future models predicting an excess of events over the SM expectation, the analyses are conducted in a model-independent way, with no optimization for a particular exotic signature. This avoids biases toward one of the many possible BSM theories. Nevertheless, in order to keep a close to optimal sensitivity to a wide range of new physics scenarios, monojet analyses can be repeated in various signal kinematic regions defined in terms of a threshold on the leading jet transverse momentum $p_T$ and on the $E_T^{\text{miss}}$ in the event. Both the ATLAS and CMS analyses chose four different signal regions, the definition of which are presented in Table 2.

## 2. Determination of the Standard Model Background

### 2.1. *Motivation for data-driven techniques*

Although many new physics searches concentrate on final states where the SM contribution is expected to be small, it is worth scrutinizing phase space regions with high SM background. As illustrated in Fig. 1, the $E_T^{\text{miss}}$ distribution of models with extra dimensions, and of generic dark matter models, is similar to the $E_T^{\text{miss}}$ distribution of the SM contribution to monojet events. Phase space selections for which the SM background is negligible would therefore yield negligible signal. Hence, a strategy to find new physics in samples with large SM backgrounds is required. This is not impossible; the Higgs after all has been found in such an environment.[34,35] The key to retain the potential for discovery in such situations is the ability to obtain a precise determination of the SM background.

As mentioned in Sec. 1, the QCD multijet background in jets + $E_T^{\text{miss}}$ events is negligible due to the excellent hermiticity of the ATLAS and CMS detectors, which results in a low probability to mis-measure a high $p_T$ jet. In supersymmetric squark or UED Kaluza–Klein-quark pair production, as well as in generic dark matter or large extra dimensions searches, only one or two hard jets are produced in the event, while extra softer jets can come from radiation. To maximize the sensitivity to these events without suffering from large top-quark background, a veto on events with at least three jets can be applied.[b] In order to further suppress the SM backgrounds in

[b]A low-$p_T$ second jet is tolerated to avoid large suppression of the phase-space acceptance.

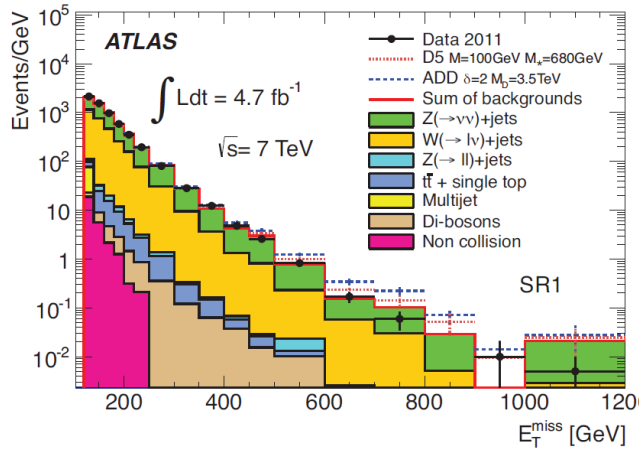


Fig. 1. $E_T^{\text{miss}}$ distribution for the various SM contributions to monojet final state compared to the $E_T^{\text{miss}}$ distribution for two examples of new physics: graviton production in the ADD large extra dimensions scenario, and direct dark matter production in generic effective dark matter model. The $E_T^{\text{miss}}$ distribution of these new physics scenarios is similar to the corresponding distribution for the total SM background to monojets events.

the monojet signal regions, events with reconstructed and identified charged leptons (electron or muon) are vetoed. The residual SM contribution to monojet events will therefore mostly come from a $W$ or a $Z$ boson produced in association with jets ($> 90\%$). The largest and irreducible background consists of $Z(\nu\nu)$+jets events. The second largest, reducible, contribution is due to the events consisting of a $W$ boson plus a jet, where the charged lepton from the $W$ decay is not reconstructed, or, in the case where it is a tau lepton decaying hadronically, results in additional low $p_T$ jets. These backgrounds are altogether referred to as the "electroweak background."

The implementation of the physics processes involving the strong interaction in event generators includes various approximations and the use of phenomenological models, while our modeling of the detector effects on final states involving jets is far from being perfect in hadron colliders. These effects inevitably result in large systematic uncertainties on the predictions of $W/Z$ + jets background extracted from Monte Carlo simulation. For example, such predictions are affected by renormalization and factorization scale uncertainties on the $W/Z$ + jets cross-sections, as well as by uncertainties on the nonperturbative QCD modeling of the Parton Density Functions (PDF), on the jet-parton matching scheme, and on the fragmentation and hadronization models used to simulate the transition from quarks to jets. The largest experimental uncertainties include the effect on the prediction due to the jet energy scale and resolution, uncertainties on the modeling of the pile-up, and the uncertainty on the luminosity calculation. These uncertainties introduce serious limitations to the potential for discovery of signal embedded in a large background.

Well-defined $W$ + jets and $Z$ + jets data events with fully reconstructed and identified leptons can be used to model the main SM backgrounds to monojet events

within high accuracy. The idea is that in these $W/Z$ + jets events, the jets have the same topology and kinematic distributions as in the electroweak background to monojet events, while the $E_T^{\text{miss}}$ distribution can be obtained after a proper removal of the charged leptons. By a proper normalization of the distributions obtained from the selected events, the electroweak background to monojet events can be accurately determined. Such techniques, which directly use data to model the physics processes of interest, are called "data-driven" background determinations. They typically suppress the systematic uncertainties resulting from the simulation-based predictions, and consequently improve the sensitivity to new physics. The following section presents a brief overview of the use of such techniques as employed by the ATLAS collaboration in its latest published monojet analysis (for a more detailed review of the techniques, see review on the subject in Ref. 30).

### 2.2. *Determination of the electroweak background*

The determination of all the electroweak backgrounds is done using exclusive data control regions (CRs) consisting of well-identified $W(\ell\nu)$ + jets or $Z(\ell\ell)$ + jets SM events satisfying the same detector-level requirements as those used to define the signal regions. The method used to obtain a monojet background estimate from them is based on "pseudo-"cross-section measurements. The jet distributions of the $W(\ell\nu)$ + jets and $Z(\ell\ell)$ + jets candidate events are first corrected to account for any of the small electroweak or QCD backgrounds contained in the CRs. The pseudo-cross-sections are obtained by correcting the residual (i.e. after background subtraction) number of events in each distribution, for the efficiency and kinematic acceptance of the lepton-related selection cuts used in the definition of the CRs. These measurements correspond to "pseudo-"cross-section measurements, because the jet kinematics are kept at the detector level. By adding to the $E_T^{\text{miss}}$ distribution the momenta of the charged leptons coming from the $W$ or $Z$ boson decays, a robust modeling of the corresponding distribution for $Z(\nu\nu)$ + jets is obtained.

The presence of reconstructed leptons in the CRs slightly distorts the shape and the normalization of the $E_T^{\text{miss}}$ and number of jets distributions, compared to what they are when the $Z$ boson decays to a pair of neutrinos. For example, removing jets associated with electrons in $Z(ee)$ + jets events removes part of the available jet phase space compared to that in $Z(\nu\nu)$ + jets events. Similarly, additional radiation from muons and electrons in the CRs can produce extra jets that would not be present in $Z(\nu\nu)$ + jets events. Correction factors based on simulation are used to eliminate these small differences ($\sim$10%) between control and signal region. Simulations are also used to estimate the lepton acceptance corrections, while efficiencies are typically estimated from data. The impact of the simulation-based systematic uncertainties mentioned above on the precision of the overall electroweak background prediction is small: these corrections are obtained through ratios of simulated events where the same jets and $E_T^{\text{miss}}$ selection cuts are applied to both the numerator and the denominator of the simulation-based correction factor.

This leads to an almost complete cancellation of QCD and jet effects. In the end, simulation is only used to correct for lepton acceptance and QED radiation effects, in order to normalize the jet distributions obtained from the data CRs to those in signal regions. To obtain the final determination of the $Z(\nu\nu)+\text{jets}$ background to monojet events, the already corrected $Z+\text{jets}$ pseudo-cross-sections must be multiplied by a factor of 5.94 to account for the difference between $Z(\ell\ell)$ and $Z(\nu\nu)$ branching ratios.

In order to obtain an estimate of the $W(\ell\nu)+\text{jets}$ background, a similar procedure is applied to the $W+\text{jets}$ CRs. However, instead of applying a correction factor related to the QED radiation of the lepton and the factor of 5.94 mentioned above, the full lepton phase space of the $W+\text{jets}$ pseudo-cross-section must be corrected for the small probability that the charged leptons from the $W$ decay escape detection. In such case, the event survives the tight lepton vetoes used to suppress this reducible $W+\text{jets}$ background. Ratios of simulated events with the same jets and $E_T^{\text{miss}}$ selections are once again used in order to obtain such probabilities of surviving the vetoes without suffering from large systematic uncertainties.

The $W+\text{jets}$ CRs can also be used, together with a precise SM measurement of the $W+\text{jets}$ to $Z+\text{jets}$ cross-sections ratio (as was done, for example, by the ATLAS collaboration[36]), to obtain other independent determination of the $Z(\nu\nu)+\text{jets}$ background to monojet events. The background estimate from all of these CRs ($Z(ee)+\text{jets}$, $Z(\mu\mu)+\text{jets}$, $W(e\nu)+\text{jets}$ and $W(\mu\nu)+\text{jets}$) can be combined, taking correlations into account, to improve the overall precision of the monojet background prediction.

In summary, the method to determine the $W/Z+\text{jets}$ background to monojet events can be described in four steps:

(1) Selection of events in data CRs, $N^{\text{data}}$, where the same jets and $E_T^{\text{miss}}$ requirements (accounting for the leptons momenta) that are used to define the monojet data sample, are applied;
(2) Subtraction of other electroweak, top and QCD backgrounds, $N_{\text{bkg}}$, in each of these data CRs;
(3) Correcting for the lepton acceptance $A$, and efficiency $\epsilon$. This provides the pseudo-cross-sections used for the prediction;
(4) Correcting for the presence of the leptons in the CRs and the difference between $Z(\ell\ell)$ and $Z(\nu\nu)$ branching ratios to get the $Z(\nu\nu)+\text{jets}$ background prediction; or applying the probability of losing the lepton in the $W$ CRs, to determine the $W+\text{jets}$ background to monojet events. This correction factor is denoted by $C$ in Eq. (1).

For example, $Z(\nu\nu)+\text{jets}$ is determined from $Z(\ell\ell)+\text{jets}$ CR as follows:

$$N^{\text{SR}}_{Z(\nu\nu)+\text{jets}} = \frac{\left(N^{\text{Data}}_{Z(\ell\ell)+\text{jets}} - N_{\text{bkg}}\right)}{A_{\ell\ell} \times \epsilon_{\ell\ell}} \times C\,. \tag{1}$$

Steps (2)–(4) determine the proper normalization to be applied to the raw CR distributions used to determine the background. However, as mentioned above, the QED effects distort the $E_T^{\text{miss}}$ distribution, in addition to scaling it. Lepton efficiency and backgrounds in the CRs can also vary depending on the kinematic of the events. In order to recover the most accurate model of the $E_T^{\text{miss}}$ distribution for the $Z(\nu\nu) + \text{jets}$ and the $W(\ell\nu) + \text{jets}$ contribution to monojet events, all the correction factors must be computed in bins of the $E_T^{\text{miss}}$ distribution obtained in the CR. Equation (1) thus takes a different value in each bin of this distribution.

In Eq. (1), it is assumed that the same trigger is used to collect data in the control and signal region. This is the case, for example, in the muon-based CRs. However, a different trigger is used in the electron-based CRs. A correction for the difference in trigger efficiencies and luminosities of the two data samples must be applied. The ratios of these efficiencies and luminosities are typically close to unity and known to high accuracy, with small uncertainty.

### 2.3. *Determination of the residual background*

QCD multijet events slightly contribute to the signal regions even if they are highly suppressed by a large $E_T^{\text{miss}}$ selection cut and by the requirement of an azimuthal angle separation, between the jets and the $E_T^{\text{miss}}$ ($|\Delta\phi(E_T^{\text{miss}}, \text{jet})| > 0.5$ in the ATLAS monojet analysis), or between the leading jet and the second jet ($|\Delta\phi(\text{1st jet, 2nd jet})| < 2.5$ in the CMS analysis). Such a small residual QCD contribution is mainly due to the complete loss of one or more jets resulting in large fake $E_T^{\text{miss}}$. This background cannot be properly estimated by simulation, and data-driven techniques must instead be used. Data CRs are defined by applying all the signal selections except the cut on the azimuthal separation between $E_T^{\text{miss}}$ and the jets (in the case of the ATLAS analysis), which is reversed in order to have an enriched QCD CR. Extrapolating the $p_T$ of the jet along the $E_T^{\text{miss}}$ below the 30 GeV jet definition threshold gives an estimate of the number of events in which a jet is completely lost and thus an estimate of the multijet background.[29,30]

There is also a contribution from noncollision background, which mainly includes cosmic and beam halo events. This background, being less than 2%, is estimated using data-driven techniques that strongly depend on the detector and the location of the accelerator (for details of the techniques used by ATLAS, see Ref. 37). Finally, there is a small contribution from single top, $t\bar{t}$ and diboson events. These backgrounds can be estimated from simulation with no impact on the accuracy of the overall background prediction.

## 3. Results

### 3.1. *Experimental results*

Using the techniques discussed in Sec. 2, the ATLAS and CMS collaborations obtained a robust SM background determination for each of their different signal

Table 3. Breakdown of the ATLAS SM background predictions for monojet events, and comparison with data passing the selection requirements for various jet $p_T$ and $E_T^{\text{miss}}$ thresholds. The data sample corresponds to an integrated luminosity of 4.7 fb$^{-1}$. The total uncertainty quoted is the quadratic sum of statistical and systematic uncertainties.[30]

| | SR1 | SR2 | SR3 | SR4 |
|---|---|---|---|---|
| Processes | Events | | | |
| $Z \to \nu\nu + \text{jets}$ | $63000 \pm 2100$ | $5300 \pm 280$ | $500 \pm 40$ | $58 \pm 9$ |
| $W \to \tau\nu + \text{jets}$ | $31400 \pm 1000$ | $1853 \pm 81$ | $133 \pm 13$ | $13 \pm 3$ |
| $W \to e\nu + \text{jets}$ | $14600 \pm 500$ | $679 \pm 43$ | $40 \pm 8$ | $5 \pm 2$ |
| $W \to \mu\nu + \text{jets}$ | $11100 \pm 600$ | $704 \pm 60$ | $55 \pm 6$ | $6 \pm 1$ |
| $t\bar{t} + \text{single } t$ | $1240 \pm 250$ | $57 \pm 12$ | $4 \pm 1$ | — |
| QCD multijets | $1100 \pm 900$ | $64 \pm 64$ | $8^{+9}_{-8}$ | — |
| Noncoll. background | $575 \pm 83$ | $25 \pm 13$ | — | — |
| $Z/\gamma^* \to \tau\tau + \text{jets}$ | $421 \pm 25$ | $15 \pm 2$ | $2 \pm 1$ | — |
| Di-bosons | $302 \pm 61$ | $29 \pm 5$ | $5 \pm 1$ | $1 \pm 1$ |
| $Z/\gamma^* + \text{jets}$ | $204 \pm 19$ | $8 \pm 4$ | — | — |
| Total background | $124000 \pm 4000$ | $8800 \pm 400$ | $750 \pm 60$ | $83 \pm 14$ |
| Events in data (4.7 fb$^{-1}$) | 124703 | 8631 | 785 | 77 |

Table 4. Breakdown of the CMS SM background predictions for monojet events, and comparison with data passing the selection requirements for various $E_T^{\text{miss}}$ thresholds. The data sample corresponds to an integrated luminosity of 5.0 fb$^{-1}$. The total uncertainty quoted is the quadratic sum of statistical and systematic uncertainties.[31]

| $E_T^{\text{miss}}$ [GeV/$c$] | $> 250$ | $> 300$ | $> 350$ | $> 400$ |
|---|---|---|---|---|
| Processes | Events | | | |
| $Z(\nu\nu) + \text{jets}$ | $5106 \pm 271$ | $1908 \pm 143$ | $900 \pm 94$ | $433 \pm 62$ |
| $W + \text{jets}$ | $2632 \pm 237$ | $816 \pm 83$ | $312 \pm 35$ | $135 \pm 17$ |
| $t\bar{t}$ | $69.8 \pm 69.8$ | $22.6 \pm 22.6$ | $8.5 \pm 8.5$ | $3.0 \pm 3.0$ |
| $Z(\ell\ell) + \text{jets}$ | $22.3 \pm 22.3$ | $6.1 \pm 6.1$ | $2.0 \pm 2.0$ | $0.6 \pm 0.6$ |
| Single $t$ | $10.2 \pm 10.2$ | $2.7 \pm 2.7$ | $1.1 \pm 1.1$ | $0.4 \pm 0.4$ |
| QCD Multijets | $2.2 \pm 2.2$ | $1.3 \pm 1.3$ | $1.3 \pm 1.3$ | $1.3 \pm 1.3$ |
| Total SM | $7842 \pm 367$ | $2757 \pm 167$ | $1225 \pm 101$ | $573 \pm 65$ |
| Data | 7584 | 2774 | 1142 | 522 |

regions outlined in Table 2. The results are presented in Tables 3 and 4. A good agreement is observed between data and the SM predictions for both monojet analyses and in all the defined signal regions, with differences between the predictions and the observations smaller than the total uncertainty on the background estimate. This agreement is not only limited to the number of events expected in the signal regions, but it also applies to the full $E_T^{\text{miss}}$ distributions, as can be seen in Fig. 1 for

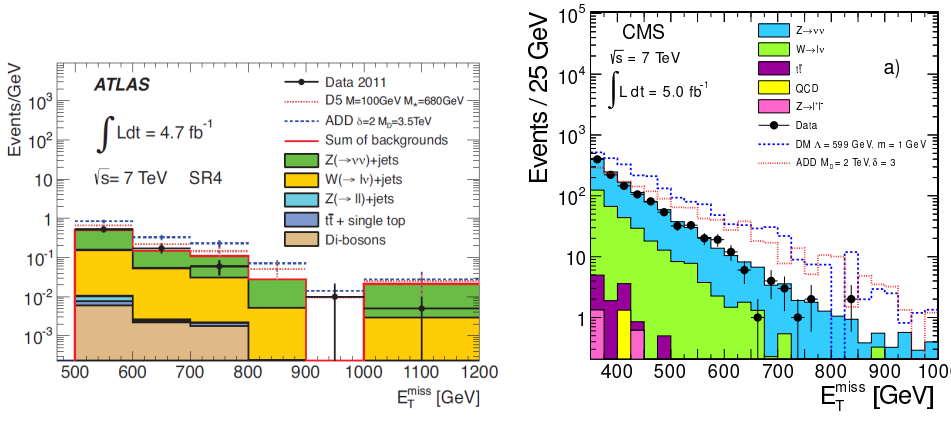


Fig. 2. Left: Comparison of the data-driven SM background estimate for the $E_T^{\text{miss}}$ distribution with data, in the SR4 ($p_T^{\text{jet}} > 500$ GeV, $E_T^{\text{miss}} > 500$ GeV) ATLAS signal region.[30] Right: Comparison of the data-driven SM background estimate for the $E_T^{\text{miss}}$ distribution with data, in the SR3 ($p_T^{\text{jet}} > 110$ GeV, $E_T^{\text{miss}} > 350$ GeV) CMS signal region.[31] In both cases, the agreement between the predictions and the observation is good.

the first ATLAS kinematic signal region, the one which has the highest statistics. Similar conclusions apply to all the signal regions tested by both experiments, as can be seen on the left panel of Fig. 2 for the example of the highest ATLAS kinematic region, and on the right panel of the same figure for an intermediate CMS kinematic region.

While these results do not give evidence for new physics in the LHC monojet data, they can be used to constrain new physics scenarios predicting signal in this final state. To calculate the upper limits on the signal yield, both collaborations used the RooStats $\text{CL}_\text{S}$ prescription.[38] This produces probability density functions for the background-only and for the signal+background hypotheses, which can be used to derive confidence intervals on the signal strength. Model-independent 90% and 95% confidence level (CL) upper limits on the visible new physics cross-section, defined as the production cross-section times acceptance and efficiency, $\sigma \times A \times \epsilon$, are therefore set, and are listed in Tables 5 and 6 for the ATLAS and CMS analyses, respectively. Preliminary studies made with 10.5 $\text{pb}^{-1}$ of 8 TeV ATLAS data reveal that similar model-independent constraints can be set on the visible new physics cross-section, as can be seen in Table 7.

### 3.2. *Theoretical interpretations*

The model-independent limits presented above can further be translated to 95% CL limits on the fundamental parameters of a given new physics theory. For example, in the case of the ADD scenario of large extra dimensions, the model-independent limits can be used to constrain the fundamental Planck scale parameter $M_D$, for

Table 5. The ATLAS 90% and 95% CL model-independent expected and observed upper limits on new physics visible cross-section $\sigma \times A \times \epsilon$ (pb) in each of the four signal regions of the ATLAS 7 TeV monojet analysis.[30]

| Signal region | Expected 90% (pb) | Observed 90% (pb) | Expected 95% (pb) | Observed 95% (pb) |
|---|---|---|---|---|
| Region 1 | 1.54 | 1.63 | 1.82 | 1.92 |
| Region 2 | 0.15 | 0.13 | 0.18 | 0.17 |
| Region 3 | 0.020 | 0.026 | 0.024 | 0.030 |
| Region 4 | 0.0064 | 0.0055 | 0.0079 | 0.0069 |

Table 6. The CMS 95% CL model-independent expected and observed upper limits on new physics visible cross-section $\sigma \times A \times \epsilon$ (pb) in each of the four signal regions of the CMS 7 TeV monojet analysis.[31]

| Signal region | Expected 95% (pb) | Observed 95% (pb) |
|---|---|---|
| Region 1 | 0.156 | 0.120 |
| Region 2 | 0.065 | 0.074 |
| Region 3 | 0.040 | 0.032 |
| Region 4 | 0.0236 | 0.0190 |

Table 7. Preliminary model-independent ATLAS 95% CL expected and observed upper limits on new physics visible cross–section $\sigma \times A \times \epsilon$ (pb) in each of the four signal regions of the ATLAS 8 TeV monojet analysis.[39]

| Signal region | Expected 95% (pb) | Observed 95% (pb) |
|---|---|---|
| Region 1 | 2.6 | 2.8 |
| Region 2 | 0.16 | 0.16 |
| Region 3 | 0.04 | 0.05 |
| Region 4 | 0.03 | 0.02 |

various possible numbers of extra dimensions. To calculate such limits, the acceptance and the detecting efficiency of the graviton signal in a given kinematic region must be estimated from simulation. These estimates suffer from systematic uncertainties that were essentially eliminated from the background determinations due to the use of data-driven techniques. The constraints on the parameters of the theory are therefore weaker than those on the visible cross-sections. Signal systematic uncertainties have both experimental and theoretical sources. The experimental uncertainties include those on the jet and $E_T^{\text{miss}}$ energy scale and resolution, as well as the uncertainties on the trigger and the integrated luminosity. Theoretical uncertainties are associated with the choice of the PDF set, the modeling of the initial and final state radiation (ISR/FSR), and the choice of factorization and renormalization scales. The signal region for which the expected sensitivity to $M_D$ is the highest among the four different kinematic regions investigated by each

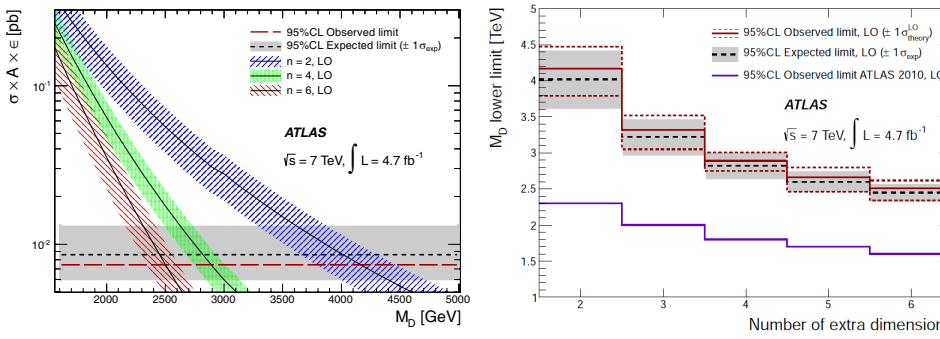


Fig. 3. (Color online) Left: Theoretical predictions for the ADD visible cross-section $\sigma \times A \times \epsilon$ obtained using the fourth ATLAS signal region SR4 as a function of $M_D$ for $n = 2$, $n = 4$ and $n = 6$ extra spatial dimensions. The bands around the ADD curves show the effect of theoretical uncertainties. For comparison, observed (segmented solid line) and expected (dashed line) 95% CL upper limits on $\sigma \times A \times \epsilon$ are both shown. The shaded areas around the expected limit indicate the sensitivity of the limits on the signal experimental systematic uncertainty.[30] Right: 95% CL lower limits on $M_D$ for different numbers of extra dimensions based on SR4. Observed and expected limits are shown as solid and dashed lines, respectively. The grey $\pm 1\sigma$ band around the expected limit represents the dependence of the limits on the statistical fluctuations and the experimental systematic uncertainties. The impact of the theoretical uncertainties is shown by the red small-dashed $\pm 1\sigma$ limits around the observed limits.[30] The first 2010 35 pb$^{-1}$ data ATLAS limits[40] are also shown for comparison.

experiment is chosen to set the limits. This corresponds to the fourth signal region in the analysis performed by ATLAS, and the third signal region in CMS.

Figure 3 presents the visible cross-section for the graviton emission of the ADD scenario, as a function of the fundamental Planck scale $M_D$, for 2, 4 and 6 extra dimensions. The red dashed horizontal line corresponds to the observed limit on the graviton emission visible cross-section obtained from the model-independent limits presented in Subsec. 3.1. The black dotted horizontal line corresponds to the expected limit, obtained by assuming that the number of observed events is exactly the same as the number of predicted events. The intersection of the predicted visible cross-section from the theory with the observed-limit line obtained from the data analysis provides the constraint on $M_D$. The shaded grey band around the horizontal expected limit indicates the range of variation of the limit occurring when the graviton signal acceptance and efficiency are varied within their experimental systematic uncertainties. The band around the theoretical visible cross-sections corresponds to the variations that could be obtained on the limits when the theory predictions are varied within their uncertainties. These bands must not be interpreted as uncertainties on $M_D$ since this quantity is not being measured. They rather represent an evaluation of the sensitivity of the limits on the modeling assumptions, both theoretical and experimental, used to derive these limits. A summary of the lower limits on $M_D$ as a function of the number of extra dimensions is provided in Fig. 3. It can be seen that the limit reaches $\sim 4.2$ TeV for $n = 2$ extra dimensions,

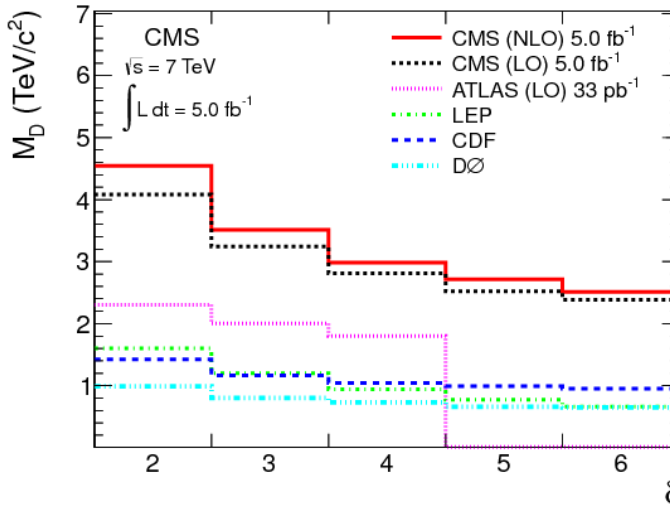


Fig. 4. (Color online) Comparison of the CMS lower limits on $M_D$ versus the number of extra dimensions[31] with the first 2010 ATLAS data (33 pb$^{-1}$) limits, as well as with LEP, CDF and D0 limits on $M_D$. The difference between the solid red line and the dotted black line shows the impact of adding NLO QCD corrections to the ADD theoretical predictions.

and $\sim 2.5$ TeV for $n = 6$. The reduction of the $M_D$ limits with increasing number of extra dimensions is a consequence of the dependence of the graviton emission cross-section[18] on $M_D$ as $\frac{2\pi^{n/2}}{\Gamma(n/2)M_D^{2+n}}$.

Comparable limits ($\sim$ 4.1 TeV for $n = 2$, $\sim$ 2.4 TeV for $n = 6$) have been obtained by the CMS collaboration, as can be seen in Fig. 4. This figure also displays the impact of adding higher-order QCD corrections (NLO) to the leading order graviton emission cross-section: it increases the limits on $M_D$ by 5%–12%, depending on the number of extra dimensions. It moreover shows that the LHC limits feature a significant improvement over the constraints imposed on $M_D$ by Tevatron results. This is mostly due to an increase in the cross-section of the graviton emission processes when the center-of-mass energy of the collision increases, as similar techniques and data samples were used for the CDF results. Increasing the center-of-mass energy of the LHC from 7 TeV to 14 TeV would further increase the ADD cross-sections by a factor of $\sim$ 15–30 for $n = 2 - 6$ extra dimensions, while the $Z(\nu\nu) + \text{jets}$ total cross-section would only increase by a factor of $\sim 4$. This would result in an overall enhancement of the sensitivity of the analysis to new physics. Preliminary sensitivity studies performed with simulation indicate that with about 100 fb$^{-1}$ of ATLAS 14 TeV data, an ADD signal could be discovered with a signal significance of five standard deviations ($5\sigma$) for values of $M_D$ as high as 9 TeV.[26] The LHC sensitivity could go even higher if extensions of the minimal ADD model are considered. As an example, if one considers supersymmetric large extra dimension scenarios, motivated by string theory, a $5\sigma$ discovery of the signal for a scalar partner of the graviton could be made for $M_D$ as high as 14 TeV.[27] Despite

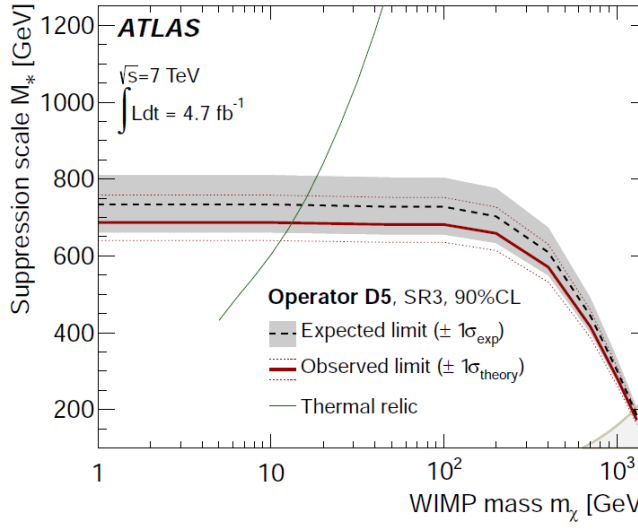


Fig. 5. (Color online) ATLAS lower limits at 90% CL on $M^*$ for different $m_\chi$. The region below the limit lines is excluded. Observed and expected limits are shown as dashed black and red solid lines, respectively. The grey $\pm 1\sigma$ band around the expected limit is the variation expected from statistical fluctuations and experimental systematic uncertainties. The impact of the theoretical uncertainties is shown by the thin red dotted $\pm 1\sigma$ limit lines around the observed limit. The $M^*$ values at which WIMPs of a given mass would result in the required relic abundance are shown as rising green lines, assuming annihilation in the early universe proceeded exclusively via the given operator. The shaded light-grey regions in the bottom right corners indicate where the effective field theory approach breaks down. The plot is based on the third signal region.[30]

the higher sensitivity to $M_D$ provided by such extended theoretical scenarios, the minimal ADD model is a better benchmark to be used to compare the sensitivity to new physics in monojet events of various experiments, as it depends on only one free parameter: $M_D$.

The visible cross-section limits presented in Subsec. 3.1 being independent of any new physics model, can also be used to constrain the WIMPs production predicted in the effective theory model discussed in Sec. 1. The ATLAS limits on the WIMP production suppression scale $M^*$ as a function of the WIMP mass $m_\chi$ are obtained from the third and fourth signal regions, depending on the type of the effective operator considered, while the CMS limits are obtained from their third signal region. The procedure to extract the limits and the sources of signal systematic uncertainties considered are the same as those used for the ADD constraints in both experiments. Independent limits have been obtained for each of the five categories of operators presented in Sec. 1. For example, the limits obtained from the 7 TeV ATLAS analysis for the D5 effective operator are shown in Fig. 5. Similarly to what is shown in Fig. 3, the shaded and dotted bands around the expected and observed limits represent the sensitivity of the limits to the experimental and theoretical uncertainties of the new physics signal predictions. The

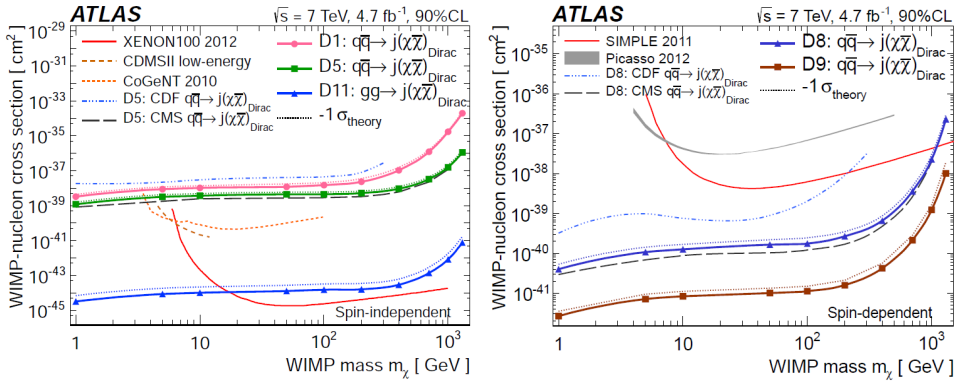


Fig. 6. The ATLAS 90% CL upper limits on spin-independent (left) and spin-dependent (right) WIMP-nucleon scattering cross-sections versus WIMP mass. The thick solid lines are the observed limits excluding signal theoretical uncertainties. The dotted lines are the limits including the theoretical uncertainties. The ATLAS limits are for the four light flavors assuming equal coupling strengths for all quark flavors to the WIMPs.[30] For comparison, 90% CL limits from the SIMPLE, Picasso, CDF and CMS experiments are also shown.[39]

light-grey shaded region in the lower right corner of the figure indicates the region of the model parameter space where the effective field theory approach for WIMP pair production breaks down.[14] The green line intersecting the limit curve on the plot represents the value of the scale $M^*$ needed in order for the effective model to predict the correct relic abundance as measured by the WMAP satellite,[2] in the absence of any other interaction than the one considered (e.g. D5). Under the assumption that dark matter is entirely composed of WIMPs, ATLAS limits on $M^*$ that are above the value required for the thermal relic density exclude the case where WIMPs annihilate exclusively to the SM particles via the corresponding operator. If thermal relic WIMPs exist in these parameter space regions above the thermal relic line, there would have to be other annihilation channels or annihilation via other operators in order to have consistent predictions with the WMAP measurements.

The lower limits on $M^*$ can further be translated to upper limits on the WIMP-nucleon scattering cross-section, as shown in Figs. 6 and 7, for the 7 TeV ATLAS and CMS analyses respectively, for both cases of spin-dependent and spin-independent WIMP-nucleon interactions.[14,30] This allows for a comparison of the limits on WIMPs obtained at the LHC from the monojet analyses, with the equivalent limits obtained from direct dark matter detection experiments. The spin-independent ATLAS limits are particularly relevant in the low $m_\chi$ region ($< 10$ GeV) where the XENON100,[41] CDMSII,[42] or CoGeNT[43] limits suffer from a kinematic suppression. The LHC spin-dependent limits are significantly better than those provided by any direct-detection experiments for sub-TeV scale WIMP masses, showing how powerful hadronic collider experiments are in dark matter searches.

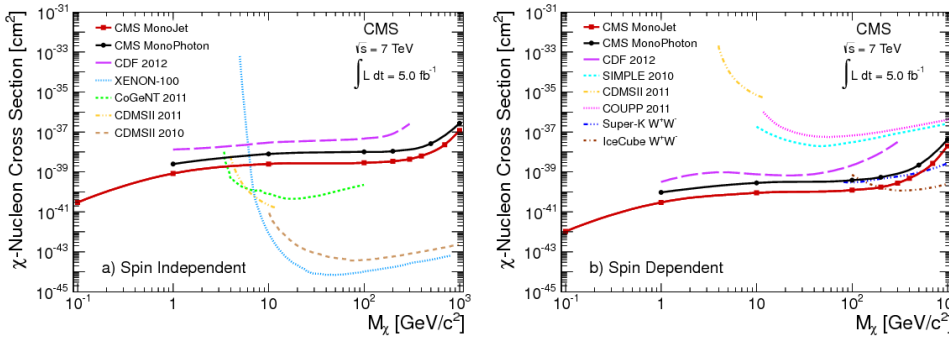


Fig. 7. Comparison of the CMS 90% CL upper limits on the dark matter-nucleon scattering cross-section versus mass of dark matter particle for the (left) spin-independent and (right) spin-dependent models[31] with results from CMS using mono photon signature, CDF, XENON100, CoGeNT, COUPP, CDMS II, Picasso, SIMPLE, Ice-Cube and Super-K collaborations.

## 4. Conclusion

Monojet events constitute one of the important final states in which dark matter can be found in hadron colliders. They also offer a great opportunity to search for quantum gravity effects at distance scales accessible to experiments. As monojet events offer rich perspective of new physics discoveries, they have been carefully studied in all hadron colliders since CERN SPS, continuing at the Tevatron and now at the energy frontier set by the LHC. The sensitivity to new physics in these events strongly depends on how precise the predictions of the SM contribution to this final state are. Simulation-based background determinations for jets + $E_T^{\text{miss}}$ final states typically suffer from large systematic uncertainties. However, precision measurements of the SM can be used in data-driven techniques to largely offset these uncertainties, and optimize the discovery potential in monojet events.

The ATLAS and CMS monojet studies performed with the 7 TeV $p$–$p$ collision data at the LHC constitute the most complete and sensitive analyses of this final state. Their results provide the state-of-the-art information that can be obtained from monojet events. They both use the data-driven techniques sketched in Sec. 2, and adopt a model-independent approach to new physics searches. As good agreement has been observed between data and the expected SM backgrounds in both analyses, the results are interpreted as upper limits on the visible cross-sections for any new physics scenario in various signal kinematic regions. These limits can further be used to constrain some BSM models that result in the monojet signature. Such models include the pair production of WIMP dark matter candidates which, based on astrophysical observations, provides one of the decisive indications for new physics in high energy physics; and graviton production in the context of ADD large extra dimensions scenario, a useful benchmark model allowing good comparison between various monojet studies. The monojet exotics physics searches performed with the ATLAS and CMS detectors can also be used to study other

interesting models such as invisible decays of the Higgs,[44] or search for unparticles.[45,46] The model-independent limits set by the ATLAS and CMS collaborations can be used to constrain these models and others yet to be made. Considering the large amount of 14 TeV LHC data to come in the next few years, search for new physics in monojet events will continue to be very exciting, keeping high hopes for a great discovery.

## References


1. H. E. Haber, B. C. Allanach and S. Grab, *J. High Energy Phys.* **1101**, 138 (2011).
2. WMAP Collab., *Astrophys. J. Suppl.* **192**, 18 (2011), arXiv:1001.4538 [astro-ph].
3. J. Feng, *J. Phys. G* **32**, R1 (2006).
4. D. H. G. Bertone and J. Silk, *Phys. Rep.* **405**, 279 (2005).
5. G. Steigman and M. S. Turner, *Nucl. Phys. B* **253**, 375 (1985).
6. H. Goldberg, *Phys. Rev. Lett.* **50**, 1419 (1983).
7. J. Ellis, J. S. Hagelin, D. V. Nanopoulos, K. Olive and M. Srednicki, *Nucl. Phys. B* **238**, 453 (1984).
8. P. M. J. Hubisz, *Phys. Rev. D* **71**, 035016 (2005).
9. G. Servant and T. Tait, *Nucl. Phys. B* **650**, 391 (2003).
10. J. L. Feng, H. C. Cheng and K. T. Matchev, *Phys. Rev. Lett.* **89**, 211301 (2002).
11. M. Beltran, D. Hooper, E. W. Kolb, Z. A. Krusberg and T. M. Tait, *J. High Energy Phys.* **1009**, 037 (2010), arXiv:1002.4137 [hep-ph].
12. A. Rajaraman, W. Shepherd, T. M. Tait and A. M. Wijangco, *Phys. Rev. D* **84**, 095013 (2011), arXiv:1108.1196 [hep-ph].
13. P. J. Fox, R. Harnik, J. Kopp and Y. Tsai, *Phys. Rev. D* **85**, 056011 (2012), arXiv:1109.4398 [hep-ph].
14. J. Goodman *et al.*, *Phys. Rev. D* **82**, 116010 (2010), arXiv:1008.1783 [hep-ph].
15. I. H. U. Baur and D. Zeppenfeld, *Int. J. Mod. Phys. A* **2**, 1285 (1987).
16. M. S. U. Baur and P. M. Zerwas, *Phys. Rev. D* **42**, 815 (1990).
17. N. Arkani-Hamed, S. Dimopoulos and G. Dvali, *Phys. Lett. B* **429**, 263 (1998), arXiv:hep-ph/9803315.
18. G. F. Giudice, R. Rattazzi and J. D. Wells, *Nucl. Phys. B* **544**, 3 (1999), arXiv:hep-ph/9811291.
19. G. Arnison *et al.*, *Phys. Lett. B* **139**, 115 (1984).
20. R. M. Barnett, H. E. Haber and G. L. Kane, *Nucl. Phys. B* **267**, 625 (1986).
21. R. M. Barnett, H. E. Haber and G. L. Kane, Implications of a systematic study of the CERN monojets for supersymmetry, SLAC-PUB-3551 LBL-18990 (1985).
22. S. D. Ellis, R. Kleiss and W. J. Stirling, *Phys. Lett. B* **167**, 464 (1986).
23. UA2 Collab., *Acta Phys. Pol. B* **17**, 795 (1986).
24. CDF Collab. (D. Acosta *et al.*), *Phys. Rev. Lett.* **92**, 121802 (2004).
25. D0 Collab. (V. M. Abazov *et al.*), *Phys. Rev. Lett.* **90**, 251802 (2003).
26. L. Vacavant and I. Hinchliffe, Model independent extra-dimension signatures with ATLAS, arXiv:0005033 [hep-ex].
27. G. Azuelos, P.-H. Beauchemin and C. P. Burgess, *J. Phys. G*: *Nucl. Part. Phys.* **31**, 1 (2005).
28. CDF Collab. (A. Abulencia *et al.*), *Phys. Rev. Lett.* **97**, 171802 (2006).
29. P.-H. Beauchemin and P. Savard, *Mod. Phys. Lett. A* **25**, 1383 (2010).
30. ATLAS Collab., Search for dark matter and large extra dimensions in events with a jet and missing transverse momentum with the ATLAS detector, Tech. Rep. ATLAS-EXOT-2011-20-003, CERN, Geneva, August, 2012, arXiv:1210.4491 [hep-ex].

31. CMS Collab., Search for dark matter and large extra dimensions in monojet events in pp collisions at $\sqrt{s} = 7$ TeV, Tech. Rep., CERN, Geneva, arXiv:1206.5663 [hep-ex].
32. CDF Collab. (T. Aaltonen *et al.*), *Phys. Rev. Lett.* **101**, 181602 (2008).
33. CDF Collab. (T. Aaltonen *et al.*), A search for dark matter in events with one jet and missing transverse energy in $p\bar{p}$ collisions at $\sqrt{s} = 1.96$ TeV, arXiv:1203.0742 [hep-ex].
34. ATLAS Collab., *Phys. Lett. B* **716**, 1 (2012).
35. CMS Collab., *Phys. Lett. B* **716**, 30 (2012).
36. ATLAS Collab., *Phys. Lett. B* **708**, 221 (2012).
37. ATLAS Collab. (D. Salek, D. Berge, J. Boyd, C. Chavez, L. Fiorini and M. Huhtinen), Beam background identification method, ATLAS-COM-DAPR-2012-001.
38. A. L. Read, *J. Phys. G* **28**, 2693 (2002).
39. ATLAS Collab., Search for new phenomena in monojet plus missing transverse momentum final states using 10 $\text{fb}^{-1}$ of pp collisions at $\sqrt{s} = 8$ TeV with the ATLAS detector at the LHC, Tech. Rep., ATLAS-CONF-2012-147, CERN, Geneva, November, 2012.
40. ATLAS Collab., *Phys. Lett. B* **705**, 294 (2011), arXiv:1106.5327 [hep-ex].
41. XENON100 Collab., Dark matter results from 225 live days of XENON100 data, arXiv:1207.5988 [astro-ph].
42. CDMS Collab., *Phys. Rev. Lett.* **106**, 131302 (2011).
43. CoGeNT Collab., *Phys. Rev. Lett.* **106**, 131301 (2011).
44. ATLAS Collab., Observing an invisibly decaying Higgs boson in ATLAS via vector boson fusion, Tech. Rep. ATL-PHYS-2003-006, CERN, Geneva, October, 2002.
45. H. Georgi, *Phys. Rev. Lett.* **98**, 221601 (2007), arXiv:hep-ph/0703260.
46. K. Cheung, W. Y. Keung and T.-C. Yuan, *Phys. Rev. D* **76**, 055003 (2007), arXiv:0706.3155 [hep-ph].